Junhao Huang

Ph.D. student
Hungarian University of
Agriculture and Life Sciences
Mechanical Engineering Doctoral School
Hungary

Ferenc Safranyik

Senior Research Fellow
Óbuda University
Donát Bánki Faculty of Mechanical and
Safety Engineering
Hungary

JánosTóth

Assistant Lecturer
Hungarian University of
Agriculture and Life Sciences
Institute of Technology
Hungary

István Keppler

Full Professor
Hungarian University of
Agriculture and Life Sciences
Institute of Technology
Hungary

Shear Test as Calibration Experiment for DEM Simulations: Sphero-polygonal Particle Model

The rapid development of computer technology provides an opportunity for researchers dealing with discrete element modeling to develop more accurate particle models. The sphero-polygonal particle model can follow the shape of the grains to be modeled much more finely. However, it is important to examine the model sensitivity to the different micromechanical parameters if we switch to the use of the sphero-polygonal model.Shear testing measurements and simulations were performed by applying the discrete element method (DEM) to find this. A geometrically more accurate sphero-polygonal particle model was applied instead of the usual sphere-clumpapproach to simulate the particle assembly's mechanical behavior during shear testing to calibrate the micromechanical parameters ofwheat grains by reproducing the shear failure curve obtained fromexperiments. Hopefully, the results will contributeto the practical applicability of the sphero-polygonal grain modeling in the discrete-elementmethod.

Keywords: *Sphero-polygonal particle, Shear test, DEM, Calibration, Sensitivity analysis.*

1. INTRODUCTION

Particle shape is a critical physical factor of DEM simulations, which directly affects the interaction [1,2] between particles and their mechanical properties [3,4]. In real particle systems, the shape of the particles may vary depending on preparation methods or external factors such as compression, abrasion, or chemical rea–ctions. These shape differences can significantly affect stress [5,6], friction properties [1,3], packing patterns [2], and contact behavior between particles. Therefore, a suitable and accurate particle shape is important for later modeling and simulations. Many scholars [7,8] prefer–red using the ellipsoidal and multi-sphere particles in DEM simulation for different purposes. In the multi-sphere model, the computation time is relatively shorter for the particle model with fewer sub-spheres than that ofhaving a larger number of sub-spheres[7,8], which indicates that the computation required to find the con–tact point between two spheres is much less than that for polygonal particles. The lack of interlocking clumps in the particle model of multi-sphere particles is one of the reasons for choosing the sphero-polygonal particle.More realistic particles improve the packing density and po–rosity accuracy in subsequent modeling and more accu–rately represent particle interlocking- and deformation behavior.In this study, the sphero-polygonal particle was utilized. The sphero-polygonal particle model com–bines the characteristics of spheres and polygons to better simulate the shape of real particles. This makes the simulation results closer to the actual situation.

Sphero-polygonal particles can adjust the shape and number of polygons as needed, thus making them closer to the shape of actual wheat particles.

DEM is a computational technique used in various fields of engineering[9], including agricultural engine–ering, to simulate the behavior of granular materials and particulate systems. Originally, DEM was developed to study soil mechanics and geotechnical engineering pro–blems [10]. But now DEM is successfully applied in a wide range of applications, not only in geotechnical engineering [11], particulate material breakage [12], and pharmaceutical processes[13] but also in analyzing the mechanical behavior of soil particles[14], and agricul–tural particles [8,14] to understand the complex inter–actions and dynamics of granular materials in agricul–tural production processes.Based on the current deve–lopment of computer hardware and software, DEM can even be used to simulate the temperature variation of granular materials[16].

In agricultural engineering, DEM serves as a valu–able tool for analyzing and optimizing various processes involving granular materials, such as grain handling [7, 17,18], storage [19,20], processing [18,21,22], soil-tool interaction, and drying [23]. By simulating the behavior of individual particles within a bulk material, DEM enables researchers and engineers to gain insights into phenomena such as particle flow [24-27], segregation [28,29], compaction [30], and mixing [28,31,32], which are critical for improving the efficiency, performance, and reliability of agricultural machinery and systems.

The direct shear test fills the shear box with granular material and then moves the box's top or bottom part in one direction at a specific speed. Data during the test can be obtained from displacement and force trans–ducers. The direct shear test is widely employed in the field of mechanical analysis for granular materials [7,

[33-35]. According to Wang et al. [36], the peak angle of the shear resistance is positively correlated with the coefficient of contact friction, and the shear resistance and the normal load also show a positive correlation based on the direct shear tests. The result by [37] emphasized that a force band connecting the upper left and lower right could affect the shear strength of the particle, and this phenomenon was also found by [36]. The advantages of the direct shear test are that it is easy, quick, and cheap compared to the triaxial shear test[35]. However, less attention has been paid todirect shear testson agricultural grains. The direct shear test wasemployed in many fields, such as interaction between the inter-group particles, geotechnical engi–neering, hydro-mechanical properties of rock fractures, and mechanical behavior of unsaturated soil [35,38-40]. Our goalsare to measure and model the effect of the wheat particle assembly's mechanical behavior by modeling the shape of the spelt wheat particle,ensuring the similarity of particle size, and calibrating these mic–romechanical parameters, the static friction coefficient, dynamic friction coefficient between particles. The main method is to conduct the numerical calibration and then run the simulations with the calibrated parameters. The following step is to perform a sensitivity analysis based on the measured shear failure envelope.

In the present work, all the simulations were carried out using the powerful commercial software package Rocky DEM [41].

This paper aims to determine the effect of the DEM micromechanical parameters on the angle of internal friction and apparent cohesion. The filling process of particulate materials can be simulated in particle mec–hanics to assist engineers in designing large-scale particle accumulation scenarios such as grain silos and the handling of construction granular material accu–mulations. In the pharmaceutical and granular food industries, designing more efficient granule conveying systems and mixing processes is possible. The men–tioned fields are related to the angle of internal friction angle and apparent cohesion. Most of the calibration methods applied in the discrete element method are also related to the analysis of macro mechanical parameters such as internal friction angle and apparent cohesion.

2. SHEAR TESTING EXPERIMENTS

The grain materialsare to be treated as an assembly of individual granulesthatinteract with each other and container or machine walls. A shear stress-strain diagram can be created based on the shear zone formed during the shear process; in addition, the shear failure envelope can be determined as $\tau = \tan\varphi \cdot \sigma + C$ (shown in fig. 1) by the measured shear stress values and the cor–responding normal stress values, where τ is shear stress, σ is the normal stress, φ is the angle of internal friction, and C is the apparent cohesion[42].The angle of internal friction and apparent cohesion are the main mechanical properties of the particle assembly in the shear failure envelope, which can be calculatedfrom the results of direct shear tests. The advantages of the direct shear test are that it is easy to use and set up equipment [35], it is possible to conduct measurements fast under different

conditions [43], and it is low-cost compared to the biaxial and triaxial tests [44]. The direct shear test, therefore, was utilized to measure the shear strength of particles at different given normal loads.
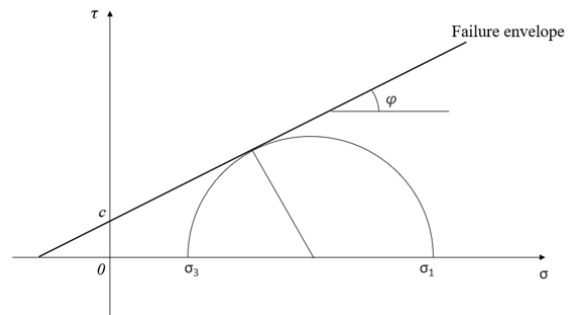

Figure 1. Shear Failure envelope with Mohr-Coulomb criterion

2.1 Shear testing technique

The standard shear test is one of the efficient techniques for buildingthe DEM modeling [45] due to it is easy to set upand explore the particle deformation and the strain, the shear force-displacement curve shows the development of the results. The Jenike shear cell [46] shown in Fig. 2 is a fundamental technique for shear testing measurement.

The shear test machine shown in Fig. 3 was utilized for our shear measurements. The shear test machine consists of several interrelated components to determine the reaction and response of the granular assemblyin the shear cell under vertical loading application, which will be shown on the screen attached to the machine. Based on the dimension of the shear box is 100x100 mm, it is important to ensure that the same amount of granular material is filled into the shear box each time, while at the same time, the shear box should not be overfilled so that the material is distributed as evenly as possible each time it is filled.
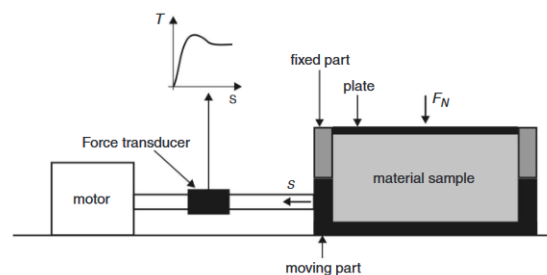

Figure 2. Jenike shear cell (Keppler et al., 2016)

Bulk density is a quite vital factor for the subsequent DEM simulation [47]. From the measurement point of view, it also deserves to be calculated with the expres–sion $\rho = m/V$. The weight of particles (m) in the shear box is measured for measuring the bulk density (ρ) due to the Volume (V) being constant at 2 L. The measured bulk density of spelt wheat particles is 755 kg/m³.
Moisture content (MC) was measured by using a moisture meter (Fig. 4) due to the MC affects the mechanical properties of the particle, such as elasticity, strength, breakage, etc. [48,49]. A given amount of the examined granular material was filled into the meter.
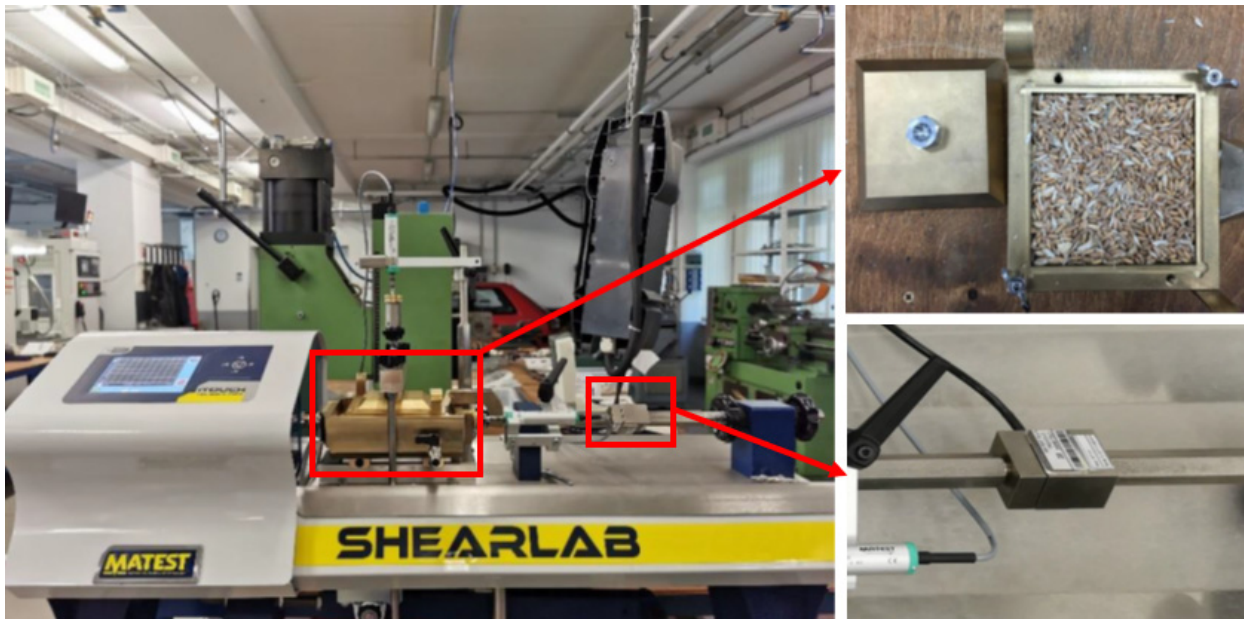
Figure 3. Shear testing machine (Right upper: Shear box; Right bottom: Force gauge)

Meanwhile, the machine measured its weight and started to heat it. The lockable plastic boxes and sealed bags were used to keep the sample clean and dry and avoid the inhomogeneity in water content for more accurate results. The moisture content is calculated automatically by the meter device. The moisture content of wheat is in the range of 15.8% to 24.65% (Table 1).

Table 1. The moisture content of wheat particles

Moisture content [%]				
I.	II.	III.	IV.	V.
18.85	15.8	19.25	24.65	24.05

Shear testing measurements were repeated 5 times under each normal stress, which was performed by converting the mass block to stress, in addition, the ratio of the measurement system is 1:10, which resulted in a 1 kg mass block corresponding to a 10 kg load. With the equation $\sigma = \dfrac{(10m) \cdot g}{A_s}$ to convert the mass to stress, where the σ is normal stress, m is the block mass, and A_s is the area of the shear cell (Table 2).

Table 2. Mass blocks converted to normal stresses

Mass block [kg]	Normal stress [kPa]
3	29.43
6	58.86
9	88.29
12	117.72

All the setting parameters could be the same, especially since the shear velocity was 1 mm/s to keep particles from breakage during the shear process, which makesthe result as accurate as possible. The shear threshold was the length at which the measurements were made.

The box moves this distance until it reaches the maximum shear force value that is going to be exerted on the material then the machine will take it back to the initial position and the results will appear in the guise of graphs of shear stress in terms of horizontal displa–cement.

Figure 4. Moisture content meter

2.2 Experimental analysis

This experiment's purpose is to illustrate the mechanical behavior of granular materials under shear and comp–ression loads by direct shear tests. Normal loads were applied to the inserted granular materials, and the particles were uniformly distributed to guarantee the accuracy of the test results.
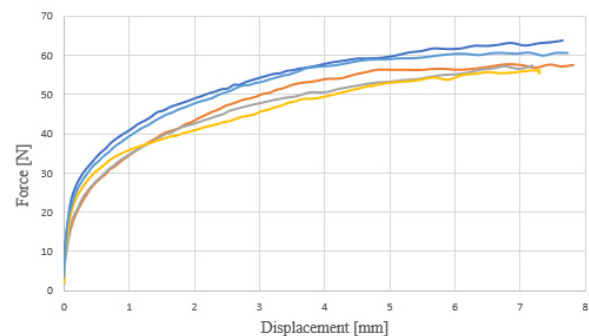

Figure 5.Diagram of the measured shear force displacement with 45 kg normal load

The measured results could be plotted in the following graph (Fig. 5) using the exact value of shear force for each corresponding displacement based on the shear zone, which has been developed inside the sample during shear measurements. As well as graphing the normal stress-shear stress relationship (Fig. 6) to produce experimental yield trends that are indicative of failure in bulk solids shear testing.

Fig. 6 is the diagram of the shear failure envelope, which shows the relationship between the shear stress vs. normal stress. Five shear test experiments were performed for each normal stress, and the data shown in the figure are not clearly visible due to the small difference between the experimentally measured shear stresses at the same normal stress. Theangle of internal friction and apparent cohesion parameterswere calculated according to the linear failure envelope approximation. According to the coefficient of determination was close to 1, the shear strength of the particles obtained from the experimental results fitted well compared to the theoretical value. Shear stress increases with increasing normal load, which is consistent with results obtained from the diagram [50].The coefficient of x in the linear regression equation represents the angle of internal friction, with a larger coefficient indicting a larger angle of internal friction (in all cases, the angle of internal friction is less than 90°). The magnitude of apparent cohesion is the value of an approximate linear line intersecting the y-axis.
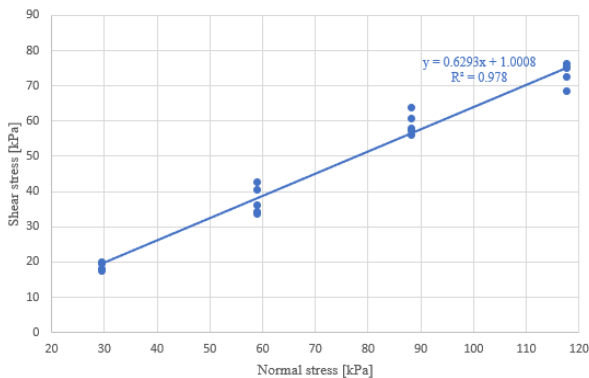

Figure 6.Measured failure envelope of shear stresses in terms of normal stresses

Taking the angle of internal friction and apparent cohesion as the macroscopic responses, a similar model is established through Rocky DEM software(Rocky DEM, 2022). Then, the particles' micromechanical parameters are calibrated to reach the optimal input micromechanical parameters. Finally, the calibration results will be validated by comparing the experimental results with the simulated results.

3.   SHEAR TEST MODELING

DEM is a numerical technique [41]for computing and collecting particle collisions and motionwith a chosen contact model. The amount of computing required by DEM restricts the simulation's runtime or the number of particles [33]. In this paper, DEM was applied to calibrate the micromechanical parameters of spelt wheat by reproducing the shear line of the particles.

This technique means another approach to examine the behavior of particulate grains through DEM simulation, which provides information on the reaction of granular materials at various particulate scales, from the interactions between particles individually to the strength gathered by large granular assemblies [34].

Its main feature is to continuously calculate these discrete particles in a very shorttimestepwhile consi–dering only inter-particle interactions and applying the governing equations [51]according to Newtonian II law of motion to get the interaction forces of each particle individually. In the simulation processes of DEM, the contact model plays a very important role. The contact model calculates the forces from which the particle positions can be deduced and the interaction force sys–tem resulting from collisions while taking into account the micromechanical properties of individual particles. Then, all the kinematic parameters of the whole system need to be updated until the last of the timestep[52]. The final simulation ends as soon as the preset timestep is reached. The Rocky DEM software (Rocky DEM, 2022) was utilized to perform the numerical simulation in this study.

The DEM simulation works as the following steps (Rocky DEM, 2022):
1. Set up physics and enable the proper modules.
2. Import geometries and set up motion frames for geometries.
3. Determine the material properties and intera–ctions of particle-particle and particle-boun–dary.
4. Choose a proper input and determine the simulation region.
5. Start the simulation.
6. DEM software does the following:

$$\sum F_{net} = \sum F_{body} + \sum F_{surface} = m \cdot \frac{d_v}{d_t} \qquad (1)$$

(a) Locate all neighboring particles and boundaries with which will contact with each other;
(b) Calculate the sum of all forces acting on the particle:

$$v_{new} = v_{old} + \int_{t}^{\tau+\Delta t} \frac{\sum F_{net}}{m} \cdot dt \qquad (2)$$

(c) The DEM software applies the present particle position, velocity, and timestep to shift it to the following position within the simulation:

$$x_{new} = x_{old} + \int_{t}^{\tau+\Delta t} v_{new} \cdot dt \qquad (3)$$

(d) Repeat the simulation until the last timestep is reached.

3.1 Governing equations of discrete element modeling

In Rocky DEM software, there are optional choices for the contact force model. However, in this paper, the Hertzian [53] spring-dashpot model was employed for

the normal contact force calculation procedure, and the Mindlin-Deresiewicz[53] was used for the tangential contact force calculation procedure. The Hertz-Mindlin model is widely applied in the shear testing simulation based on the publications [54]. In addition, the Coulomb law combined with the static friction coefficient limits the tangential force [55]. The damping components we–re concluded in both normal and tangential forces; besides, the damping coefficient is related to the coefficient of restitution [55].In this paper, the adhesive force model was not applied since there is no adhesion between particles. The stiffness coefficient K_H in the normal contact force model:

$$K_H = \frac{4}{3} E^* \sqrt{R^*} \tag{4}$$

The normal contact force equation employed the re–duced Young's modulus and the effective or equivalent radius. The reduced Young's modulus E^* is:

$$\frac{1}{E^*} = \frac{1-v_1^2}{E_1} + \frac{1-v_2^2}{E_2} \tag{5}$$

The E_1 and E_2 are the Young's moduli of the two contacting particles or the particle and the boundary, and the v_1 and v_2 are the Poisson's ratios, respectively, depending on the contacting type (Rocky DEM, 2022). The equivalent radius R^* can be defined as:

$$\frac{1}{R^*} = \begin{cases} \dfrac{2}{L_1} + \dfrac{2}{L_2} \text{ for particle-particle collison} \\ \dfrac{2}{L} \text{ for particle-boundary collison} \end{cases} \tag{6}$$

The L_1 and L_2 are the sizes of the contacting particles in a particle-particle collision, and the L is the size of the particle in a particle-boundary collision (Rocky DEM, 2022). For the damping part for the Hertzian model in Rocky DEM, the damping coefficient is defined as:

$$C_H = 2\eta_H \sqrt{m^* K_H} \tag{7}$$

where m^* is the effective mass:

$$\frac{1}{m^*} = \begin{cases} \dfrac{1}{m_1} + \dfrac{1}{m_2} \text{ for particle-particle collison} \\ \dfrac{1}{m} \text{ for particle-boundary collison} \end{cases} \tag{8}$$

The m_1 and m_2 are the masses of the contacting particles, and m is the mass of the particle contacting with the boundary. The damping ratio η_H for the Hert–zian spring-dashpot model is defined as:

$$\eta_H = \frac{\sqrt{5}}{2} \eta \tag{9}$$

where the η is the same damping ratio used in the linear spring-dashpot model (Rocky DEM, 2022).

The expression of the Hertzian spring-dashpot model in Rocky DEM can refer to:

$$F_n = K_H s_n^{\frac{3}{2}} + C_H S_n^{\frac{1}{4}} \dot{s}_n \tag{10}$$

The tangential force model can be expressed as below:

$$F_\tau = -\mu F_n \left(1 - \zeta^{\frac{3}{2}}\right) \frac{s_\tau}{|s_\tau|} + \eta_\tau \sqrt{\frac{6\mu m^* F_n}{s_{\tau,\max}}} \zeta^{\frac{1}{4}} \dot{S}_\tau \tag{11}$$

$$\zeta = 1 - \frac{\min\left(|s_\tau|, s_{\tau,\max}\right)}{s_{\tau,\max}} \tag{12}$$

where μ is the friction coefficient utilized in the equation, F_n is the normal force as the previous equation showed, s_τ is the relative displacement regarding tan–gential, $\dot{s}_\tau$ is the relative velocity regarding tangential component, $s_{\tau,\max}$ is the maximum tangential relative displacement, m^* is the equivalent mass, and η_τ is the tangential damping ratio for this model, which is expressed in Rocky DEM by means of (Rocky DEM, 2022):

$$\eta_\tau = -\frac{\ln \varepsilon}{\sqrt{\ln^2 \varepsilon + \pi^2}} \tag{13}$$

where ε is the coefficient of the restitution for the inte–raction of the respective materials. The value of the ma–ximum relative tangential displacement $s_{\tau,\max}$ is written as:

$$s_{\tau,\max} = \mu \left(\frac{1-v_1}{2-v_1} + \frac{1-v_2}{2-v_2}\right)^{-1} s_n \tag{14}$$

where s_n is the normal overlap (Rocky DEM, 2022).

DEM calibration of micromechanical parameters is the way of systematically modifying the relevant input parameters to reproduce the dynamic behavior as observed in the laboratory experiments of the particle assembly. The angle of internal friction, angle of repose (AoR), and bulk density of particles as the macro indicators to calibrate the micromechanical parameters [56-59]. The results obtained from calibration can clo–sely modelthe macroscopic dynamic behavior of particle assembly[59].

3.2 Sphero-polygonal particles

In this study, the spelt wheat particle was used to con–duct the shear testing experiments. The particle model, therefore, referred to the shape and size of this spelt wheat particle. The particle shape and size play a very important role [5,40,52,60,61] in the simulation due to they could directly affect the input parameters that have a significant influence on the output of the simulation. Similarly, they [62] found that the angle of internal friction was also affected by the particle size.

Meanwhile, the particle size was inversely propor–tional to the density and porosity of the particle [63].

However, their studies [62] and [64] reported that the expansion of granular samples was affected by changes in normal stress but not by shape.It can reproduce the flow and accumulative behavior with high accuracy by modeling the soybean seeds as a multi-sp–here model [8]. They [26] performed multi-sphere (Fig. 7a, 7b)modeling of sunflower seeds, and the simulation

results were significantly affected by the multi-sphere model of sunflower seeds. The apparent cohesion has a clear inverse proportional relationship with the size of the particle due to the increased surface area per unit mass at the smaller size of the particle [65]. The particle in this study was modeled as a sphero-polygonal type (Fig. 7c) simplified based on the real particle shape. As we can see in Fig. 7(d), the shape of the particle is somehow regular.

Table 3. Dimensions of the spelt wheat particle

Spelt wheat particle		
Height	Width	Thickness
10.13 mm	3.66mm	2.54 mm

Of course, there were some other parameter modifications to make the shape of the modeled particle quite close to the real particle shape. The vertical aspect ratio was set to 2.65, the horizontal aspect ratio was set to 0.65, and the number of corners was set to 6 regarding the particle shape. The dimensions of the spelt wheat particle shown in Table 3, according to the real particle size of spelt wheat particle height, width, and depth, are 10.13mm, 3.66mm, and 2.54mm, respectively, 3.8 mm 100% cumulative sieve size was used for the particle size to match with the real particle size, and the 3.6mm size particle was also applied with 20% from the cumulative point of view. In order to make the filling of particles as random as the real filling process, the random angle of orientation was set to 3 radians for each of the *xyz* directions, respectively. The purpose of this is to ensure that the particles in each direction are completely random in the case of asymmetric particles.

3.3 Calibration of the micromechanical parameters

The calibration of micromechanical parameters is one of the key ways to find out the accurate parameters for future simulations successfully. Micromechanical para–meters play a very important role in discrete element modeling. Interactions between particles and between particles and boundaries are also affected by micro–mechanical parameters. Many scholars [52,66-68] conducted the calibration of input micromechanical parameters by combining the physical experiments and DEM simulations. Coetzee and Els[69] accurately predicted containerresistance's general tendency by stu–dying particles' surface energy through DEM simu–lations. Cleary [3] quantitatively discussed the effect of particle shape on the velocity, volume fraction, particle temperature, and stress distribution of the channel with DEM simulations, respectively. Su et al. [67]determined micromechanical parameters such as the shear modulus, restitution coefficient, critical normal stress, and shear stress of corn to ensure the accurate simulation ofthe corn particle crushing process. The calibration method was widely applied in various fields of the agricultural industry[19,67,70], the pharmaceutical industry(Gao et al., 2021), and geotechnics [38,71].
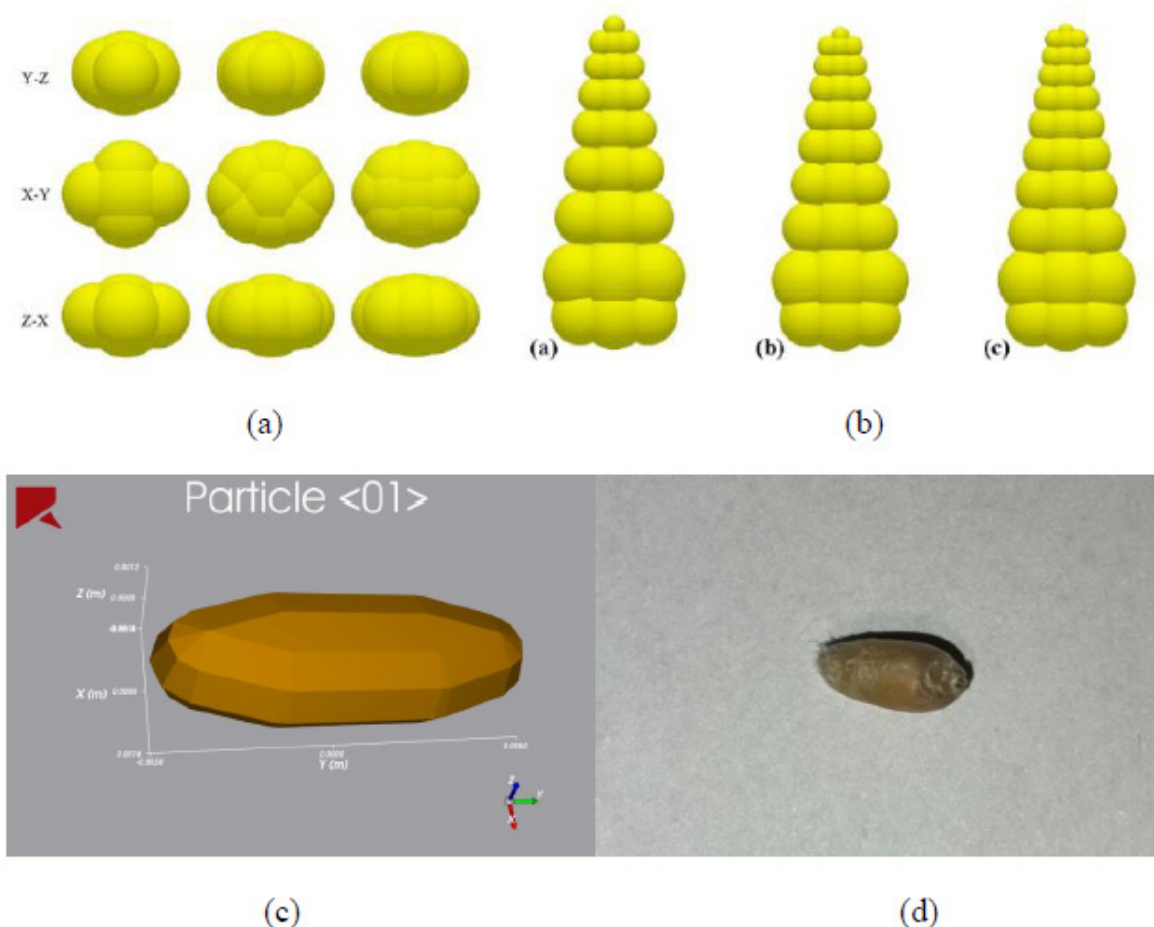

(a)

(b)

(c)

(d)

Figure 7. (a) The modeled multi-sphere of soybean seeds [8]; (b) The modeled multi-sphere of sunflower seeds [26]; (c) The modeledsphero-polygonal of the wheat particle; (d) The real wheat particle

The angle of internal friction and apparent cohesion are two response factors that represent the accuracy of the modeling. These parameters can be visualized very well in shear failure envelope curves. The tangent to the angle of internal friction is the slope of a line [72], and the extension of the line intersects the y-axis, so the distance from the origin to the intersection reflects the value of apparent cohesion. If the input micromecha– nical parameters are correct, then theoretically, we can obtain simulation results that are very close to the experimental results, i.e., the angle of internal friction and the apparent cohesion are very close to the experi– mental results so far as to equal the experimental results.

4. SHEAR TEST SIMULATION

The modeled shear cell dimensionis 100 x 50 mm. The periodic domain was used in order to reduce the simu– lation time. The ratio of shear cell edge length to par– ticle size was bigger than 8, which met the requirement of the ratio of particle size to a container [57]. This ensured that the particles could be free to move and interact with each other inside the shear box. The lid of the shear box used in the discrete element simulations was rectangular modified based on the shear tests. The sphero-polygonal shape particle was chosen in the simulations. The simulation procedures for conducting the shear test modeling are listed below.

1). Enable the stress statistical function and import the shear box geometries into the simulation zone.

2). Fill particles into the shear box with Volume Fill to make sure that the proper amount of particle filling. The single particles fall onto each other under the gravity acceleration to form the particle assembly.

3). Slowly move down the compression lid with a constant velocity to have a pre-compression after the particle assembly achieves a motionless state due to its vibration during the packing phase. The weight of the lid was designed to have a corresponding constant normal stress acting on the particle assembly.

4). Wait for the particle assembly to stabilize

5). Start the shear simulation. The lower apparatus of the shear box was slowly and at a constant speed moved toward the specified horizontal direction.
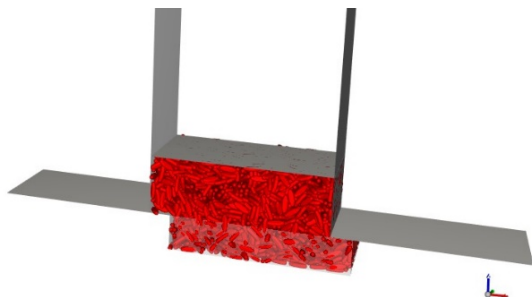
6). The shear process stops after 13 seconds.

Figure 8.DEM shear test simulation

The Stresses function recorded the time-correspon– ding shear force during the simulation (Fig. 8). The maximum shear force was converted to shear stress, which was used for plotting the failure envelope. Based on Fig. 9, it can be seen that the shear failure envelope

with calibrated micromechanical parameters is close to the measured one, which indicates the calibrated micro– mechanical parameters are accurate.
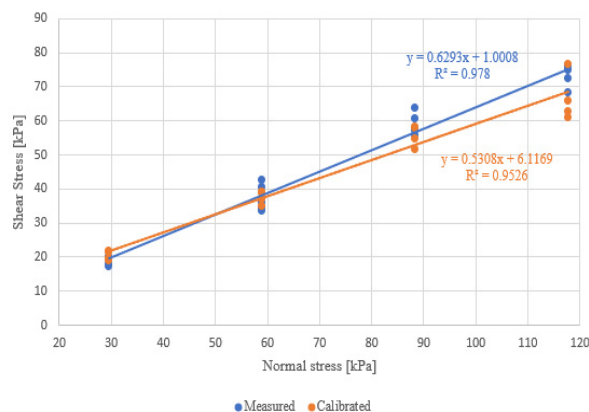

Figure 9. Measured and calibrated failure envelopes of clear spelt wheat

5. SENSITIVITY ANALYSIS

In this chapter, the micromechanical parameters were changed systematically to conduct the sensitivity test of theinternal friction angle and apparent cohesion in DEM simulations. The calibrated micromechanical parameter values are listed in Table 4. For sensitivity analysis, the multiplier values of those micromechanical parameters were also listed in Table 5.

Table 4. Calibrated micromechanical parameters

Variable	Sign	Value	Unit
Particle Young'smodulus	E	1.1e+09	N/m^2
Particle Poisson's ratio	v	0.4	-
Particle-particle static friction	μ_s	1.3	-
Particle-particle dynamic friction	μ_d	0.1	-

Table 5. Different variables with different multiplier

No.	Variable	Multiplier
1		0.5
2		0.75
3	E	1
4		1.25
5		1.5
6		0.5
7		0.75
8	v	1
9		1.25
10		1.5
11		0.5
12		0.75
13	μ_s	1
14		1.25
15		1.5
16		0.5
17		0.75
18	μ_d	1
19		1.25
20		1.5

5.1 Particle-particle dynamic friction

The particle-particle dynamic friction does not signi–ficantly affectthe angle of internal friction and the appa–rent cohesion.

5.2 Particle Poisson's ratio

Fig. 10 shows that the particle Poisson's ratio does not affect significantly the angle of internal friction. And the particle Poisson's ratio has no effect on the apparent cohesion.
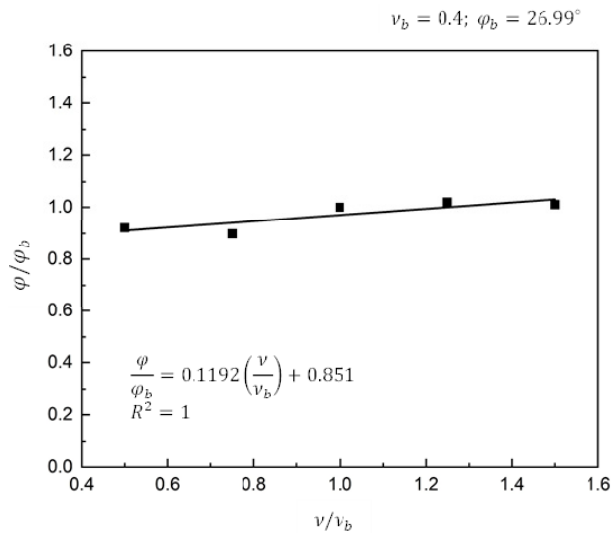

$$v_b = 0.4; \quad \varphi_b = 26.99°$$

$$\frac{\varphi}{\varphi_b} = 0.1192\left(\frac{v}{v_b}\right) + 0.851$$
$$R^2 = 1$$

Figure 10. The effect of particle Poisson's ratio on the angle of internal friction

5.3 Particle-particle static friction

Fig. 11 and Fig. 12 show the effect of particle-particle static friction on the angle of internal friction and appa–rent cohesion. Both the angle of internal friction and the apparent cohesion increase with increasing friction between particles. The tendency to increase the angle of internal friction is relatively small. However, the increasing trend of apparent cohesion is very significant.
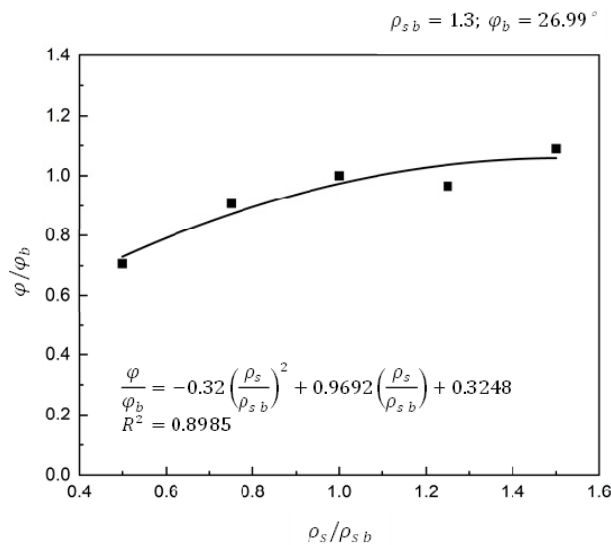

$$\rho_{sb} = 1.3; \quad \varphi_b = 26.99°$$

$$\frac{\varphi}{\varphi_b} = -0.32\left(\frac{\rho_s}{\rho_{sb}}\right)^2 + 0.9692\left(\frac{\rho_s}{\rho_{sb}}\right) + 0.3248$$
$$R^2 = 0.8985$$

Figure 11. The effect of particle-particle static friction on the angle of internal friction

$$\rho_{sb} = 1.3; \quad c_b = 5.5493$$

$$\frac{c}{c_b} = 1.9943\left(\frac{\rho_s}{\rho_{sb}}\right)^2 - 1.9911\left(\frac{\rho_s}{\rho_{sb}}\right) + 1.1263$$
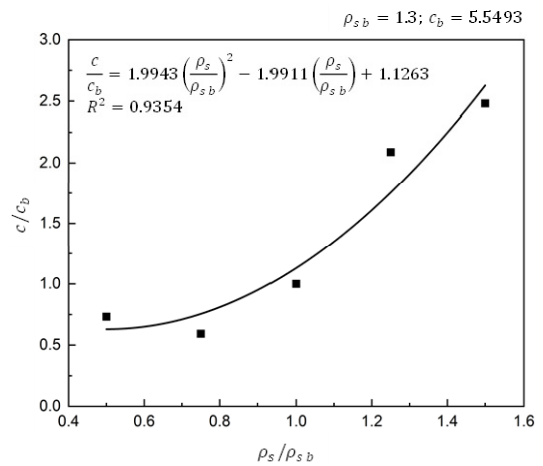$$R^2 = 0.9354$$

Figure 12. The effect of particle-particle static friction on the apparent cohesion

5.4 Particle Young's modulus

It can be seen based on the Fig. 13 and Fig. 14, that the angle of internal friction increases with increasing the particle Young's modulus, but the trend is not so strong. The particle Young's modulus has no effect on the apparent cohesion. The results are completely in contrast with their research [42]. This is probably because the particles' distinct shapes caused completely different results.
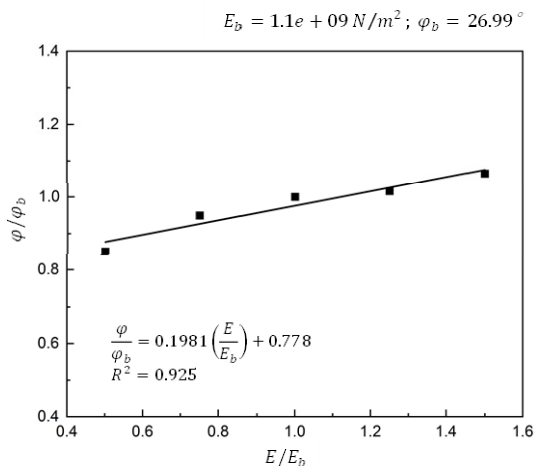

$$E_b = 1.1e + 09 \, N/m^2; \quad \varphi_b = 26.99°$$

$$\frac{\varphi}{\varphi_b} = 0.1981\left(\frac{E}{E_b}\right) + 0.778$$
$$R^2 = 0.925$$

Figure 13. The effect of particle Young's modulus on the angle of internal friction

$$E_b = 1.1e + 09 \, N/m^2; \quad c_b = 5.5493$$

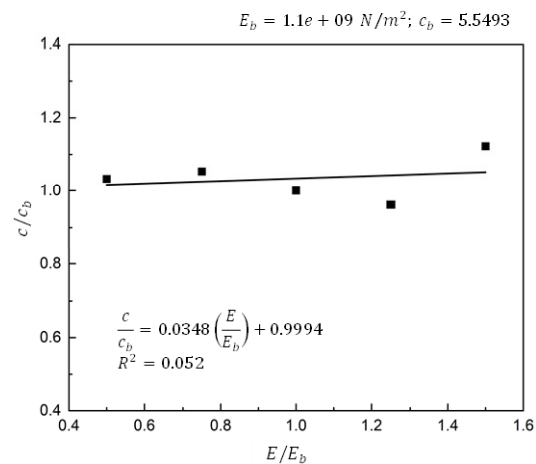$$\frac{c}{c_b} = 0.0348\left(\frac{E}{E_b}\right) + 0.9994$$
$$R^2 = 0.052$$

Figure 14. The effect of particle Young's modulus on the apparent cohesion

4. CONCLUSION

The result of the experimental shear test could be reproduced by conducting the shear test simulations with calibrated micromechanical parameters. The sensitivity analysis of micromechanical parameters was performed by modeling and drawing the shear failure envelope at each level of various multipliers. The sphero-polygon particle shape could cause different results regarding the angle of internal friction and apparent cohesion. The following could be concluded based on the above shear test simulations:

1). Particle-particle dynamic friction shows that does not have any effect on the angle of internal friction and the apparent cohesion.

2). Particle Poisson's ratio has almost no effect on the angle of internal friction and the apparent cohesion based on our conducted simulations. The detailed equation regarding the effect on the angle of internal friction is shown below.

$$\frac{\varphi}{\varphi_b} = 0.1192\left(\frac{v}{v_b}\right) + 0.851 \tag{15}$$

3). The angle of internal friction increases with the increase in particle-particle static friction; meanwhile, the particle-particle static friction significantly affects the particle apparent cohesion with a positive proportional relationship. Two equations are shown below, respectively.

$$\frac{\varphi}{\varphi_b} = -0.32\left(\frac{\rho}{\rho_{sb}}\right)^2 + 0.9692\left(\frac{\rho_s}{\rho_{sb}}\right) + 0.3248 \tag{16}$$

$$\frac{c}{c_b} = 1.9943\left(\frac{\rho_s}{\rho_{sb}}\right)^2 - 1.9911\left(\frac{\rho_s}{\rho_{sb}}\right) + 1.1263 \tag{17}$$

4). The particle Young's modulus has some effect on the angle of internal friction angle of the particles, but not a particularly large one. And the particle Young's modulus has a negligible effect on the apparent cohesion. The different effects are noticed in the following two equations.

$$\frac{\varphi}{\varphi_b} = 0.1981\left(\frac{E}{E_b}\right) + 0.778 \tag{18}$$

$$\frac{c}{c_b} = 0.0348\left(\frac{E}{E_b}\right) + 0.9994 \tag{19}$$

The different particle models could lead to totally distinct effects on the angle of internal friction and apparent cohesion. That means the particle models play a pivotal role in DEM simulations, becoming increasingly crucial in future research. Accurate particle modeling ensures the fidelity of simulated interactions, aiding in understanding complex granular behavior. The correct representation of particles in simulations enhances predictive capabilities, allowing for insights into phenomena. As DEM continues to develop, advancements in particle modeling techniques will be indispensable for tackling diverse engineering and scientific challenges associated with granular materials. The increasing complexity of particle models in DEM simulations leads to a substantial rise in simulation time and costs.

DECLARATION OF COMPETING INTEREST

The authors declare that they have no known competing financial interests or personal relationships that could have appeared to influence the work reported in this paper.

REFERENCES

[1] A. Danesh, A. A. Mirghasemi, M. Palassi, "Evaluation of particle shape on direct shear mechanical behavior of ballast assembly using discrete element method (DEM)," *Transp. Geotech.*, vol. 23, p. 100357, Jun. 2020, doi: 10.1016/j.trgeo.2020.100357.

[2] J. Härtl, J. Y. Ooi, "Numerical investigation of particle shape and particle friction on limiting bulk friction in direct shear tests and comparison with experiments," *Powder Technol.*, vol. 212, no. 1, pp. 231–239, Sep. 2011, doi: 10.1016/j.powtec.2011.05.022.

[3] P. W. Cleary, "The effect of particle shape on simple shear flows," *Powder Technol.*, vol. 179, no. 3, pp. 144–163, Jan. 2008, doi: 10.1016/j.powtec.2007.06.018.

[4] J. Horabik, M. Molenda, "Parameters and contact models for DEM simulations of agricultural granular materials: A review," *Biosyst. Eng.*, vol. 147, pp. 206–225, Jul. 2016, doi: 10.1016/j.biosystemseng.2016.02.017.

[5] G. Rong, G. Liu, D. Hou, C. Zhou, "Effect of Particle Shape on Mechanical Behaviors of Rocks: A Numerical Study Using Clumped Particle Model," *Sci. World J.*, vol. 2013, pp. 1–12, 2013, doi: 10.1155/2013/589215.

[6] T. Zhang, C. Zhang, J. Zou, B. Wang, F. Song, W. Yang, "DEM exploration of the effect of particle shape on particle breakage in granular assemblies," *Comput. Geotech.*, vol. 122, p. 103542, Jun. 2020, doi: 10.1016/j.compgeo.2020.103542.

[7] K. Sun *et al.*, "A DEM-based general modelling method and experimental verification for wheat seeds," *Powder Technol.*, vol. 401, p. 117353, Mar. 2022, doi: 10.1016/j.powtec.2022.117353.

[8] J. Xu, X. Wang, Z. Zhang, W. Wu, "Discrete Element Modeling and Simulation of Soybean Seed Using Multi-Spheres and Super-Ellipsoids," *IEEE Access*, vol. 8, pp. 222672–222683, 2020, doi: 10.1109/ACCESS.2020.3044656.

[9] S. W. Lommen, D. L. Schott, G. Lodewijks, "Multibody dynamics model of a scissors grab for co-

simulation with discrete element method," *FME Trans.*, vol. 40, no. 4, pp. 177–180, 2012.

[10] P. A. Cundall, O. D. L. Strack, "A discrete nume–rical model for granular assemblies," *Géotechnique*, vol. 29, no. 1, pp. 47–65, Mar. 1979, doi: 10.1680/geot.1979.29.1.47.

[11] A. Grabowski, M. Nitka, "3D DEM simulations of basic geotechnical tests with early detection of shear localization," *Stud. Geotech. Mech.*, vol. 43, no. 1, pp. 48–64, Dec. 2020, doi: 10.2478/sgem-2020-0010.

[12] T. Afshar, M. M. Disfani, A. Arulrajah, G. A. Narsilio, S. Emam, "Impact of particle shape on breakage of recycled construction and demolition aggregates," *Powder Technol.*, vol. 308, pp. 1–12, Feb. 2017, doi: 10.1016/j.powtec.2016.11.043.

[13] Y. Gao, G. De Simone, M. Koorapaty, "Calibration and verification of DEM parameters for the quantitative simulation of pharmaceutical powder compression process," *Powder Technol.*, vol. 378, pp. 160–171, Jan. 2021, doi:10.1016/j.powtec.2020.09.019.

[14] P. Wang, Z.-Y. Yin, "Effect of particle breakage on the behavior of soil-structure interface under con–stant normal stiffness condition with DEM," *Com–put. Geotech.*, vol. 147, p. 104766, Jul. 2022, doi: 10.1016/j.compgeo.2022.104766.

[15] S. Adilet *et al.*, "Calibration Strategy to Determine the Interaction Properties of Fertilizer Particles Using Two Laboratory Tests and DEM," *Agricul–ture*, vol. 11, no. 7, 2021, doi: 10.3390/agriculture 11070592.

[16] T. Mitterlehner, G. Kartnig, M. Haider, "Analysis of the thermal ratcheting phenomenon in packed-bed thermal energy storage using Discrete Element Method," *FME Trans.*, vol. 48, no. 2, pp. 427–431, 2020, doi: 10.5937/fme2002427M.

[17] Z. Ma, Y. Li, L. Xu, "Discrete-element method si–mulation of agricultural particles' motion in vari–able-amplitude screen box," *Comput. Electron. Agric.*, vol. 118, pp. 92–99, Oct. 2015, doi: 10.1016/j.compag.2015.08.030.

[18] Y. Zeng, B. Mao, F. Jia, Y. Han, G. Li, "Modelling of grain breakage of in a vertical rice mill based on DEM simulation combining particle replacement model," *Biosyst. Eng.*, vol. 215, pp. 32–48, 2022, doi: https://doi.org/10.1016/j.biosystemseng.2021.12.022.

[19] J. Horabik *et al.*, "Calibration of discrete-element-method model parameters of bulk wheat for storage," *Biosyst. Eng.*, vol. 200, pp. 298–314, Dec. 2020, doi: 10.1016/j.biosystemseng.2020.10.010.

[20] D. G. Mogale, S. K. Kumar, F. P. G. Márquez, M. K. Tiwari, "Bulk wheat transportation and storage problem of public distribution system," *Comput. Ind. Eng.*, vol. 104, pp. 80–97, Feb. 2017, doi: 10.1016/j.cie.2016.12.027.

[21] A. G. Chiaravalle, I. M. Cotabarren, J. Piña, "DEM breakage calibration for single particle fracture of maize kernels under a particle replacement app–

roach," *Chem. Eng. Res. Des.*, vol. 195, pp. 151–165, Jul. 2023, doi: 10.1016/j.cherd.2023.05.015.

[22] Y. Su *et al.*, "A combined experimental and DEM approach to optimize the centrifugal maize brea–kage tester," *Powder Technol.*, vol. 397, p. 117008, Jan. 2022, doi: 10.1016/j.powtec.2021.11.052.

[23] J. Azmir, Q. Hou, A. Yu, "CFD-DEM simulation of drying of food grains with particle shrinkage," *Powder Technol.*, vol. 343, pp. 792–802, Feb. 2019, doi: 10.1016/j.powtec.2018.11.097.

[24] Y. Guo, C. Wassgren, W. Ketterhagen, B. Hancock, B. James, and J. Curtis, "A numerical study of gra–nular shear flows of rod-like particles using the discrete element method," *J. Fluid Mech.*, vol. 713, pp. 1–26, 2012, doi: 10.1017/jfm.2012.423.

[25] P. Van Liedekerke, E. Tijskens, E. Dintwa, F. Rioual, J. Vangeyte, H. Ramon, "DEM simulations of the particle flow on a centrifugal fertilizer spre–ader," *Powder Technol.*, vol. 190, no. 3, pp. 348–360, Mar. 2009, doi: 10.1016/j.powtec.2008.08.018.

[26] S. Wang, Z. Yu, Aorigele, W. Zhang, "Study on the modeling method of sunflower seed particles based on the discrete element method," *Comput. Electron. Agric.*, vol. 198, p. 107012, 2022, doi: https://doi.org/10.1016/j.compag.2022.107012.

[27] S. Zhang, M. Z. Tekeste, Y. Li, A. Gaul, D. Zhu, J. Liao, "Scaling of the angle of repose test and its influence on the calibration of DEM parameters using upscaled particles," *Biosyst. Eng.*, vol. 194, pp. 196–212, Jun. 2020, doi: 10.1016/j.biosys temseng.2020.03.018.

[28] B. Jadidi, M. Ebrahimi, F. Ein-Mozaffari, and A. Lohi, "Mixing and segregation assessment of bi-disperse solid particles in a double paddle mixer," *Particuology*, vol. 74, pp. 184–199, Mar. 2023, doi: 10.1016/j.partic.2022.06.006.

[29] N. Khola, C. Wassgren, "Correlations for shear-in–duced percolation segregation in granular shear flows," *Powder Technol.*, vol. 288, pp. 441–452, Jan. 2016, doi: 10.1016/j.powtec.2015.11.003.

[30] Q. Qi, Y. Nie, X. Wang, S. Liu, "Exploring the effects of size ratio and fine content on vibration compaction behaviors of gap-graded granular mix–tures via calibrated DEM models," *Powder Tech–nol.*, vol. 415, p. 118156, Feb. 2023, doi: 10.1016/j.powtec.2022.118156.

[31] S. Garneoui, P. Korzenszky, I. Keppler, "Enhan–cement of the mixture quality of corn grains in a single-shaft paddle mixer using DEM simulations," *J. Mech. Sci. Technol.*, Feb. 2023, doi:10.1007/s12206-023-0223-1.

[32] S. Garneoui, I. Keppler, P. Korzenszky, "Mixing enhancement of wheat granules in a hopper bottom lab-scale mixer using discrete element simulations," *FME Trans.*, vol. 48, no. 4, pp. 868–873, 2020, doi: 10.5937/fme2004868G.

[33] N. Jiménez-Herrera, G. K. P. Barrios, L. M. Tava–res, "Comparison of breakage models in DEM in simulating impact on particle beds," *Adv. Powder*

Technol., vol. 29, no. 3, pp. 692–706, Mar. 2018, doi: 10.1016/j.apt.2017.12.006.

[34] I. Keppler, A. Bablena, N. D. Salman, P. Kiss, "Discrete element model calibration based on *in situ* measurements," *Eng. Comput.*, vol. 39, no. 5, pp. 1947–1961, May 2022, doi: 10.1108/EC-05-2021-0288.

[35] M. Nitka, A. Grabowski, "Shear band evolution phenomena in direct shear test modelled with DEM," *Powder Technol.*, vol. 391, pp. 369–384, Oct. 2021, doi: 10.1016/j.powtec.2021.06.025.

[36] Z. Wang, G. Jing, Q. Yu, H. Yin, "Analysis of ballast direct shear tests by discrete element method under different normal stress," *Measurement*, vol. 63, pp. 17–24, Mar. 2015, doi: 10.1016/j.measurement.2014.11.012.

[37] H. Huang, E. Tutumluer, "Discrete Element Modeling for fouled railroad ballast," *Constr. Build. Mater.*, vol. 25, no. 8, pp. 3306–3312, Aug. 2011, doi: 10.1016/j.conbuildmat.2011.03.019.

[38] L. Zou, V. Cvetkovic, "A new approach for predicting direct shear tests on rock fractures," *Int. J. Rock Mech. Min. Sci.*, vol. 168, p. 105408, Aug. 2023, doi: 10.1016/j.ijrmms.2023.105408.

[39] J. Larsson, F. Johansson, D. Mas Ivars, E. Johnson, M. Flansbjer, and N. W. Portal, "A novel method for geometric quality assurance of rock joint replicas in direct shear testing – Part 2: Validation and mechanical replicability," *J. Rock Mech. Geotech. Eng.*, p. S1674775523000100, Jan. 2023, doi: 10.1016/j.jrmge.2022.12.012.

[40] X. Liu, A. Zhou, K. Sun, S.-L. Shen, "Discrete element modelling of the macro/micro-mechanical behaviour of unsaturated soil in direct shear tests including wetting process," *Powder Technol.*, vol. 415, p. 118125, Feb. 2023, doi: 10.1016/j.powtec.2022.118125.

[41] "Rocky DEM," 2022.

[42] I. Keppler, F. Safranyik, I. Oldal, "Shear test as calibration experiment for DEM simulations: a sensitivity study," *Eng. Comput.*, vol. 33, no. 3, Jan. 2016, doi: 10.1108/EC-03-2015-0056.

[43] G. Alhakim, C. Núñez-Temes, J. Ortiz-Sanz, M. Arza-García, L. Jaber, M. L. Gil-Docampo, "Experimental application and accuracy assessment of 2D-DIC in meso-direct-shear test of sandy soil," *Measurement*, vol. 211, p. 112645, Apr. 2023, doi: 10.1016/j.measurement.2023.112645.

[44] A. Qian, Y. Ding, H. Lu, Y. Wu, "Numerical simulation of direct shear tests on gas hydrate-bearing sediments using the discrete element method," *Gas Sci. Eng.*, vol. 114, p. 204995, Jun. 2023, doi: 10.1016/j.jgsce.2023.204995.

[45] D18 Committee, *Test Method for Shear Testing of Bulk Solids Using the Jenike Shear Cell*. doi: 10.1520/D6128-14.

[46] A. W. Jenike, "Storage and flow of solids," *Bull. No 123 Utah State Univ.*, 1964.

[47] I. Mishra, M. J. Molnar, M. Y. Hwang, A. Shetty, C. M. Hrenya, "Experimental validation of the extraction of a particle-particle cohesion model (square-force) from simple bulk measurements (defluidization in a rheometer)," *Chem. Eng. Sci.*, vol. 259, p. 117782, Sep. 2022, doi: 10.1016/j.ces.2022.117782.

[48] Y. Han *et al.*, "Breakage behaviour of single rice particles under compression and impact," *Adv. Powder Technol.*, vol. 32, no. 12, pp. 4635–4650, Dec. 2021, doi: 10.1016/j.apt.2021.10.017.

[49] W. Kruszelnicka, P. Leda, A. Tomporowski, K. Ambrose, "Breakage behavior of corn kernels subjected to repeated loadings," *Powder Technol.*, vol. 435, p. 119372, Feb. 2024, doi: 10.1016/j.powtec.2024.119372.

[50] N. Mashhadiali, F. Molaei, "Theoretical and experimental investigation of a shear failure model for anisotropic rocks using direct shear test," *Int. J. Rock Mech. Min. Sci.*, vol. 170, p. 105561, Oct. 2023, doi: 10.1016/j.ijrmms.2023.105561.

[51] A. Bablena, N. Schrempf, I. Keppler, "The effect of particle shape on the angle of repose test based calibration of discrete element models," *Hung. Agric. Eng.*, no. 40, pp. 39–46, 2021, doi: 10.17676/HAE.2021.40.39.

[52] F. Safranyik, A. Varga, I. Oldal, I. Keppler, "Optimal and effective technique for particle packing," *Adv. Powder Technol.*, vol. 31, no. 8, pp. 3222–3235, Aug. 2020, doi: 10.1016/j.apt.2020.06.016.

[53] A. Di Renzo, F. P. Di Maio, "An improved integral non-linear model for the contact of particles in distinct element simulations," *Chem. Eng. Sci.*, vol. 60, no. 5, pp. 1303–1312, Mar. 2005, doi: 10.1016/j.ces.2004.10.004.

[54] J. Nečas *et al.*, "Shear lid motion in DEM shear calibration and the effect of particle rearrangement on the internal friction angle," *Powder Technol.*, vol. 403, p. 117417, May 2022, doi: 10.1016/j.powtec.2022.117417.

[55] L. M. Tavares, V. A. Rodriguez, M. Sousani, C. B. Padros, J. Y. Ooi, "An effective sphere-based model for breakage simulation in DEM," *Powder Technol.*, vol. 392, pp. 473–488, Nov. 2021, doi: 10.1016/j.powtec.2021.07.031.

[56] M. Mousaviraad, M. Z. Tekeste, K. A. Rosentrater, "Calibration and Validation of a Discrete Element Model of Corn Using Grain Flow Simulation in a Commercial Screw Grain Auger," *Trans. ASABE*, vol. 60, no. 4, pp. 1403–1415, 2017, doi: 10.13031/trans.12200.

[57] C. J. Coetzee, "Calibration of the discrete element method and the effect of particle shape," *Powder Technol.*, vol. 297, pp. 50–70, Sep. 2016, doi: 10.1016/j.powtec.2016.04.003.

[58] H. Zhou, Z. Hu, J. Chen, X. Lv, N. Xie, "Calibration of DEM models for irregular particles based on experimental design method and bulk experiments," *Powder Technol.*, vol. 332, pp. 210–223, Jun. 2018, doi: 10.1016/j.powtec.2018.03.064.

[59] X. Song, F. Dai, F. Zhang, D. Wang, Y. Liu, "Calibration of DEM models for fertilizer particles based on numerical simulations and granular experiments," *Comput. Electron. Agric.*, vol. 204, p. 107507, Jan. 2023, doi: 10.1016/j.compag.2022.107507.

[60] [60] J. M. Ting, L. Meachum, J. D. Rowell, "Effect of particle shape on the strength and deformation mechanisms of ellipse shaped granular assemblages," *Eng. Comput.*, vol. 12, no. 2, pp. 99–108, Feb. 1995, doi: 10.1108/02644409510799497.

[61] T. Roessler, A. Katterfeld, "Scaling of the angle of repose test and its influence on the calibration of DEM parameters using upscaled particles," *Powder Technol.*, vol. 330, pp. 58–66, May 2018, doi:10.1016/j.powtec.2018.01.044.

[62] M. Talafha, I. Oldal, "The effect of Triple Particle sizes on the mechanical behaviour of granular materials using Discrete element method (DEM)," *FME Trans.*, vol. 50, no. 2, pp. 139–148, 2022, doi: 10.5937/fme2201139T.

[63] V. Bharath, D. H. Ashita, V. Auradi, M. Nagaral, "Influence of variable particle size reinforcement on mechanical and wear properties of alumina reinforced 2014Al alloy particulate composite," *FME Trans.*, vol. 48, no. 4, pp. 968–978, 2020, doi: 10.5937/fme2004968B.

[64] M. Talafha, I. Oldal, S. Garneoui, "Study the particle size impact on the mechanical behaviour of granular material by discrete element method," *FME Trans.*, vol. 50, no. 3, pp. 473–483, 2022, doi: 10.5937/fme2203473T.

[65] J. J. Fitzpatrick, T. Iqbal, C. Delaney, T. Twomey, M. K. Keogh, "Effect of powder properties and storage conditions on the flowability of milk powders with different fat contents," *J. Food Eng.*, vol. 64, no. 4, pp. 435–444, Oct. 2004, doi: 10.1016/j.jfoodeng.2003.11.011.

[66] J.-Q. Zhong, L.-M. Tao, S.-P. Li, B. Zhang, J.-Y. Wang, Y.-L. He, "Determination and interpretation of parameters of double-bud sugarcane model based on discrete element," *Comput. Electron. Agric.*, vol. 203, p. 107428, Dec. 2022, doi: 10.1016/j.compag.2022.107428.

[67] Y. Su *et al.*, "Determination and interpretation of bonded-particle model parameters for simulation of maize kernels," *Biosyst. Eng.*, vol. 210, pp. 193–205, Oct. 2021, doi: 10.1016/j.biosystemseng.2021.08.022.

[68] P. Tahmasebi, "A state-of-the-art review of experimental and computational studies of granular materials: Properties, advances, challenges, and future directions," *Prog. Mater. Sci.*, vol. 138, p. 101157, Sep. 2023, doi: 10.1016/j.pmatsci.2023.101157.

[69] C. J. Coetzee, D. N. J. Els, "The numerical modelling of excavator bucket filling using DEM," *J. Terramechanics*, vol. 46, no. 5, pp. 217–227, Oct. 2009, doi: 10.1016/j.jterra.2009.05.003.

[70] R. Fan, Q. Cui, Y. Zhang, and Q. Lu, "Analysis and calibration of parameters of buckwheat grain based on the stacking experiment," *inmateh Agric. Eng.*, pp. 467–476, Aug. 2021, doi: 10.35633/inmateh-64-46.

[71] F. P. André, L. M. Tavares, "Simulating a laboratory-scale cone crusher in DEM using polyhedral particles," *Powder Technol.*, vol. 372, pp. 362–371, Jul. 2020, doi: 10.1016/j.powtec.2020.06.016.

[72] J. Bai, B. Xie, J. Yan, Y. Zheng, N. Liu, Q. Zhang, "Moisture content characterization method of wet particles of brown rice based on discrete element simulation," *Powder Technol.*, vol. 428, p. 118775, Oct. 2023, doi: 10.1016/j.powtec.2023.118775.

ТЕСТ СМИЦАЊА КАО КАЛИБРАЦИОНИ ЕКСПЕРИМЕНТ ЗА ДЕМ СИМУЛАЦИЈЕ: МОДЕЛ СФЕРО-ПОЛИГОНАЛНИХ ЧЕСТИЦА

Џ. Хуанг, Ф. Шафрањик, Ј. Тот, И. Кеплер

Брзи развој рачунарске технологије пружа могућност истраживачима који се баве моделирањем дискретних елемената да развију прецизније моделе честица. Модел сферо-полигоналних честица може много финије пратити облик зрна која се моделирају. Међутим, важно је испитати осетљивост модела на различите микромеханичке параметре ако пређемо на употребу сферо-полигоналног модела. Мерења и симулације испитивања смицања су извршена применом методе дискретних елемената (ДЕМ) да би се ово пронашло. Геометријски тачнији модел сферо-полигоналних честица примењен је уместо уобичајеног приступа сфере-групе да би се симулирало механичко понашање склопа честица током тестирања на смицање да би се калибрирали микромеханички параметри зрна пшенице репродуковањем криве смицања добијене из експеримената. Надамо се да ће резултати допринети практичној примени моделирања сферо-полигоналног зрна у методи дискретних елемената.